Journal of Sound and Vibration 376 (2016) 48–59

Contents lists available at ScienceDirect

Journal of Sound and Vibration

journal homepage: www.elsevier.com/locate/jsvi

Indirect calibration of a large microphone array for in-duct acoustic measurements

Q. Leclère [a,*], A. Pereira [b], A. Finez [c], P. Souchotte [b]

[a] Univ Lyon, INSA-Lyon, LVA EA677, F-69621 Villeurbanne Cedex, France
[b] Laboratoire de Mécanique des Fluides et d'Acoustique, École Centrale de Lyon, 36 avenue Guy de Collongue 69134 Écully Cedex, France
[c] MicrodB, 28 Chemin du petit bois 69134 Écully Cedex, France

ARTICLE INFO

Article history:
Received 23 October 2015
Received in revised form
15 March 2016
Accepted 25 April 2016
Handling Editor: P. Joseph
Available online 8 May 2016

Keywords:
In situ array calibration
Duct modal decomposition
Flush-mounted microphone array

ABSTRACT

This paper addresses the problem of in situ calibration of a pin hole-mounted microphone array for in-duct acoustic measurements. One approach is to individually measure the frequency response of each microphone, by submitting the probe to be calibrated and a reference microphone to the same pressure field. Although simple, this task may be very time consuming for large microphone arrays and eventually suffer from lack of access to microphones once they are installed on the test bench. An alternative global calibration procedure is thus proposed in this paper. The approach is based on the fact that the acoustic pressure can be expanded onto an analytically *known* spatial basis. A projection operator is defined allowing the projection of measurements onto the duct modal basis. The main assumption of the method is that the residual resulting from the difference between actual and projected measurements is mainly dominated by calibration errors. An iterative procedure to estimate the calibration factors of each microphone is proposed and validated through an experimental set-up. In addition, it is shown that the proposed scheme allows an optimization of physical parameters such as the sound speed and parameters associated to the test bench itself, such as the duct radius or the termination reflection coefficient.

1. Introduction

The investigation of the noise generated by turbomachinery, such as ducted fans, is a common problem in the aeronautics industry. The aim is to comprehend the different noise generation mechanisms, supporting the design of more silent machines. Recently, different experimental measurement techniques based on an array of microphones have been proposed for the study of ducted noise sources. These techniques typically use a microphone array either placed outside the duct [1] or flush-mounted on the duct inner surface [2–4]. The acoustic pressure data simultaneously recorded by the array microphones are then used by acoustic imaging techniques for the reconstruction of source properties (e.g. its location, strength, directivity). Examples of such techniques applied to duct noise sources are beamforming [2,5,6] or near-field acoustical holography [7]. The phase information between microphones in the array is the basis of any acoustic imaging method. A good phase calibration of array microphones is thus essential for the accuracy of such techniques, especially in the case of pin hole mounted sensors that can exhibit significant differences between their in situ frequency responses.

* Corresponding author. Fax: +33 4 72 43 87 12.
E-mail address: quentin.leclere@insa-lyon.fr (Q. Leclère).

http://dx.doi.org/10.1016/j.jsv.2016.04.033

The problem of array calibration has been the subject of research work since the 80s by Paulraj and Kailath [8], at that time applied to the direction of arrival (DOA) estimation of competing sources. In their work [8], a procedure for a particular array structure (linear and equi-spaced sensors) is proposed for gain and phase calibration. The approach is based on the fact that for uniform linear arrays and uncorrelated sources, the array Cross Spectral Matrix (CSM) has a Hermitian Toeplitz structure. However, in real conditions the CSM deviates from a Toeplitz structure due to gain and phase errors present in measurements. The method in [8] thus seeks to estimate the gain and phase errors by recovering the CSM Toeplitz structure. A particular formulation of the approach by Paulraj and Kailath was then proposed by Sng and Li [9], with the advantage of being more simple and leading to better results. This approach was extended to 2-D uniform rectangular arrays in [10], exploiting in this case the Toeplitz–block Toeplitz structure of the unperturbed CSM. The case of general array configurations was studied by Dougherty in Ref. [11]. A technique was proposed for the phase calibration of microphone arrays using a small speaker as an idealized point source. The method is based on a theoretical propagation in free-field conditions and thus measurements must be carried out in a reflection-free environment.

Building on aforementioned work [8,9], Lowis et al. [12,13] proposed a technique for the in situ phase calibration of in-duct microphone arrays. The main limitation of these techniques is that the array microphones must be equi-spaced either axially or circumferentially in the duct. However, it is common in practice the use of array designs with a geometry other than a regular arrangement. In a more recent work, Toth and Schram [14] use an impedance tube to calibrate simultaneously multiple microphones, based on a plane wave expansion of the acoustic field, which limits the approach to a frequency below which only plane waves are propagating.

A fundamental question at the experimental set-up of in-duct measurements is how to install the microphones on the duct surface. A common practice is to place it flush-mounted at the duct inner surface, either with or without the protection grid in place. The drawback is that a spatial filtering effect due to the finite size of the membrane occurs for the measurement of pressure fluctuations associated to a turbulent boundary layer [15]. An alternative is to use a remote sensor installation, named here as pin-hole system, which allows a punctual measurement of the pressure field. The system is well described in the Appendix of Ref. [16]. A consequence of this remote installation is that the frequency response of the microphone is modified by the creation of a small cavity that acts as a Helmholtz resonator. It turns out necessary thus, to apply a correction to the acoustic pressure measured by the microphones. A specific procedure for the individual calibration of each microphone using a compression driver connected to a tube of small diameter has been designed. The procedure is presented in Ref. [16] and reviewed in the present paper for completeness. Although simple and ease to implement, the individual calibration procedure is very time consuming for installations with a large number of microphones. Another drawback is the possible lack of access to every microphone in the array once they are mounted on the test bench. The above limitations reveal the interest of having a non-local method for the array calibration.

In the present work, an alternative in situ calibration method is presented with the advantage of being less restrictive in terms of assumptions and not subjected to a particular microphone array arrangement. The method is based in the fact that the measured sound field may be decomposed onto a *known* basis, in the present paper, the duct modal basis [17,18,3,19]. A projection operator is then defined and allows the projection of measurements onto the modal basis. The main hypothesis of the approach is that the residual arising from the difference between actual and projected measurements is dominated by calibration errors. As it will be seen, the method applies to any arrangement of sensors and may be potentially generalized to any acoustic field. However, the approach being based on a modal projection operation, it is basically limited to a frequency bandwidth in which the modal decomposition is valid.

The rest of the paper is organized as follows. Section 2 reviews the principles of modal decomposition in a circular duct and describes the theory of the calibration method. Next, Section 3 presents the experimental set-up for the in-duct array measurements and the validation of the proposed calibration technique. The conclusions are drawn in Section 4.

2. Theory

2.1. Modal expansion of the acoustic pressure in the duct

The acoustic pressure field at a given frequency ω at the inner wall of a duct with a constant section and without flow can be expanded as follows

$$p(z,\theta) = \sum_{n=-\infty}^{+\infty}\sum_{s=1}^{+\infty}\left(a_{ns}e^{-jk_{zns}z} + b_{ns}e^{jk_{zns}z}\right)e^{jn\theta}, \tag{1}$$

with

$$k_{zns}^2 = \left(\frac{\omega}{c}\right)^2 - \left(\frac{Z_{ns}}{\alpha}\right)^2$$

where c is the speed of sound, α the radius of the duct, and Z_{ns} the sth root of the derivative of the first kind Bessel function of order n.

If the studied field is relatively far from any acoustic source or duct geometric singularity, then the modal expansion can be done on propagating modes only. Evanescent components, with imaginary wavenumbers k_{zns} can be discarded. In this case, a finite number N of propagating modes are considered, depending on the studied frequency, satisfying $k_{zns}^2 > 0$.

For M microphone positions, Eq. (1) can be expressed as follows

$$\mathbf{p} = \mathbf{\Phi_a a} + \mathbf{\Phi_b b} = [\mathbf{\Phi_a}\ \ \mathbf{\Phi_b}]\begin{pmatrix}\mathbf{a}\\ \mathbf{b}\end{pmatrix}, \tag{2}$$

where $\mathbf{a}$ and $\mathbf{b}$ are vectors constituted respectively of a_{ns} and b_{ns} coefficients for each microphone, columns of $\mathbf{\Phi}_a$ and $\mathbf{\Phi}_b$ stand for modal contributions of each mode to microphone positions, and $\mathbf{p}$ is the vector of acoustic pressures. The modal coefficients are obtained by inverting the modal matrix:

$$\begin{pmatrix}\mathbf{a}\\ \mathbf{b}\end{pmatrix} = [\mathbf{\Phi_a}\ \ \mathbf{\Phi_b}]^{+}\mathbf{p}, \tag{3}$$

where $\mathbf{M}^{+} = (\mathbf{M}'\mathbf{M})^{-1}\mathbf{M}'$ is the pseudo-inverse of matrix $\mathbf{M}$, this operation being potentially ill-conditioned depending on the microphone number and distribution, and on the number of modal amplitudes to be identified. It is noteworthy that the calibration approach described in this work needs modal matrices to be well conditioned and overdetermined (more microphones than modes), which can be seen as a limitation of the method. However, the post-processing that can be realized with the calibrated array also often requires this condition to be fulfilled.

2.2. Consideration of the reflection matrix

In this work, sources are considered to be located on one side of the array only, contributing to waves propagating toward $z+$ at the array location ($\mathbf{a}$ coefficients). The waves travelling toward z-($\mathbf{b}$ coefficients) are due to potential reflections of the termination of the duct on the $z+$ side. A schematic representation of the duct is given in Fig. 1. The reflection matrix of the termination of the duct relates the coefficients of incident and reflected waves [20]:

$$\mathbf{b} = \mathbf{Ra} \tag{4}$$

In the following sections of this paper, several source configurations are considered, in order to analyse in-duct acoustic fields with different modal repartitions. Practical aspects are provided in Section 3.1. Considering K source configurations, Eq. (3) for all configurations can be gathered into one single system:

$$\begin{bmatrix}\mathbf{A}\\ \mathbf{B}\end{bmatrix} = [\mathbf{\Phi_a}\ \ \mathbf{\Phi_b}]^{+}\mathbf{P}, \quad \text{with } \begin{bmatrix}\mathbf{A}\\ \mathbf{B}\end{bmatrix} = \begin{bmatrix}\mathbf{a}_1, \ldots \mathbf{a}_K\\ \mathbf{b}_1, \ldots \mathbf{b}_K\end{bmatrix} \text{ and } \mathbf{P} = [\mathbf{p}_1, \ldots \mathbf{p}_K] \tag{5}$$

Considering several source configurations as in Eq. (5), the reflection matrix, $\mathbf{R}$, must satisfy the following system:

$$\mathbf{B} = \mathbf{RA} \tag{6}$$

It is thus obtained inverting matrix $\mathbf{A}$

$$\mathbf{R} = \mathbf{BA}'(\mathbf{AA}')^{-1} \tag{7}$$

Note that the calculation of $\mathbf{R}$ can be done only if matrix ($\mathbf{AA}'$) is invertible. One necessary condition is that the number of propagating modes has to be lower than the number of configurations. For a fixed number of configurations, the number of propagating modes increasing with the frequency, there will always be a frequency above which the identification of the reflection matrix will not be possible anymore. Once $\mathbf{R}$ is estimated, the modal projection can be reformulated as follows

$$\mathbf{p} = \mathbf{\Phi_a a} + \mathbf{\Phi_b Ra} = (\mathbf{\Phi_a} + \mathbf{\Phi_b R})\mathbf{a} \tag{8}$$

The interest of taking into account the reflection matrix, for modal identification approaches, is that the number of modal amplitudes to be identified is divided by a factor 2, improving the robustness of the inversion.

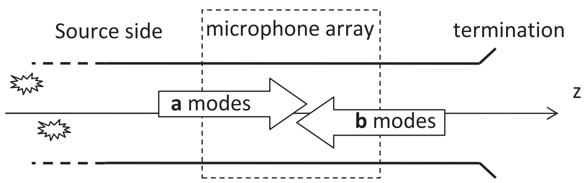

Fig. 1. Schematic representation of the duct.

2.3. Modal projection operator

The pressure vector measured by the microphone array can be projected on the subspace spanned by duct modes. The projection matrix, noted $\mathbf{\Psi}$, is defined by

$$\tilde{\mathbf{p}} = \mathbf{\Phi a} = \mathbf{\Phi \Phi}^{+}\mathbf{p} = \mathbf{\Psi p}, \tag{9}$$

where $\mathbf{\Phi}$ is the modal matrix either including or not the reflection matrix. The reconstruction error $\mathbf{n}$, representing the difference between the measured pressure vector and its modal approximation, is obtained by

$$\mathbf{n} = \mathbf{p} - \tilde{\mathbf{p}} = (\mathbf{I} - \mathbf{\Psi})\mathbf{p} \tag{10}$$

The adequacy between measurements and the modal matrix can be quantified through a the following indicator:

$$\mathrm{snr} = 20\,\log_{10}\left(\frac{\|\tilde{\mathbf{p}}\|}{\|\mathbf{n}\|}\right) \tag{11}$$

2.4. Identification of the relative sensitivity

The incident pressure on a microphone i, noted p_i, is related to its output tension, noted u_i through a potentially frequency dependent calibration factor c_i:

$$p_i(\omega) = c_i(\omega)u_i(\omega) \tag{12}$$

where ω is the cyclic frequency (rad/s). This single relation is moved to a diagonal system of equations when dealing with several microphones:

$$\mathbf{p} = \mathbf{Cu} \tag{13}$$

where the frequency dependency is omitted for the sake of simplicity. The calibration factors are supposed to be unchanged for different operating conditions. If K configurations are considered, K systems of equations are gathered in a matrix form:

$$\mathbf{P} = \mathbf{CU} \quad \text{where } \mathbf{P} = \left[\mathbf{p}_1 \ \ \mathbf{p}_2 \ \ \ldots \ \ \mathbf{p}_K\right] \text{ and } \mathbf{U} = [\mathbf{u}_1 \ \ \mathbf{u}_2 \ \ \ldots \ \ \mathbf{u}_K] \tag{14}$$

each column of which constituting equation (13) for one configuration. The absolute determination of $\mathbf{C}$ from $\mathbf{U}$ and $\mathbf{\Psi}$ (the modal basis projector) is not possible without any additional information about the overall level, or without the a priori knowledge of the calibration factors of a part of the considered sensors. However, a relative calibration can be estimated, representative of the differences in gain and phase of the different microphones. The normalized calibration factors are defined as follows:

$$d_i = c_i/\overline{c}, \quad \text{with } |\overline{c}| = \frac{1}{n}\sum_{i=1}^{n}|c_i|, \tag{15}$$

where $\overline{c}$ is an unknown scaling factor whose estimation is discussed in Section 2.6. This definition results in the following constraint on $\mathbf{D}$:

$$\frac{1}{n}\sum_{i=1}^{n}|d_i| = 1 \tag{16}$$

The scaling factor is also used to define a normalized acoustic pressure matrix $\mathbf{Q} = \mathbf{P}/\overline{c}$. A normalized version of Eq. (14) is thus

$$\mathbf{Q} = \mathbf{DU} \tag{17}$$

In our case, both $\mathbf{Q}$ and $\mathbf{D}$ are unknown, and $\mathbf{U}$ is the tension delivered by the microphones. The main hypothesis of the present approach is that $\mathbf{Q}$ should be expandable on the modal basis of the duct, the idea is thus to search for the normalized calibration vector (diagonal of $\mathbf{D}$) minimizing the modal projection error defined in the previous section. This problem can be written as follows

$$\mathbf{D}_{\mathrm{opt}} = \underset{D}{\operatorname{argmin}}\|\mathbf{DU} - \mathbf{\Psi DU}\|_F^2$$
$$\text{subject to } \frac{1}{n}\sum_{i=1}^{n}\left|\mathbf{D}_{i,i}\right| = 1 \text{ and } \mathbf{D}_{i,j} = 0 \ \forall i \neq j, \tag{18}$$

where $\|\mathbf{M}\|_F$ stands for the Frobenius norm of matrix $\mathbf{M}$. An iterative procedure is proposed in the following to solve this constrained minimization problem. The initial calibration factors are adjusted to a constant value:

$$\mathbf{D}^{(1)} = \frac{1}{n}\mathbf{I} \tag{19}$$

At iteration k, the vectors of normalized pressures are obtained by

$$\mathbf{Q}^{(k)} = \mathbf{D}^{(k)}\mathbf{U}, \tag{20}$$

where $\mathbf{U}$ and $\mathbf{Q}^{(k)}$ are, respectively, the matrices of measured tensions and normalized acoustic pressures, the columns of which correspond to the different source configurations. Then, the modal projection technique described in Section 2.3 is used to separate the normalized pressure vector in a physical part, expendable on acoustical modes, and a residual part attributed to calibration error. The physical part is given by

$$\tilde{\mathbf{Q}}^{(k)} = \mathbf{\Psi}\mathbf{Q}^{(k)}, \tag{21}$$

This *cleaned* version of the normalized acoustic pressures is then used to estimate, for each microphone, the normalized calibration factor. The following system is considered for microphone #i:

$$\tilde{\mathbf{Q}}_i^{(k)} = \mathrm{d}_i\mathbf{U}_i \tag{22}$$

where $\tilde{\mathbf{Q}}_i^{(k)}$ is the ith line of matrix $\tilde{\mathbf{Q}}^{(k)}$, $\mathbf{U}_i$ the ith line of matrix $\mathbf{U}$ (i.e. the tension from microphone i for all source configurations). The normalized calibration d_i is assessed by a least squares estimator:

$$\tilde{d}_i^{(k)} = \tilde{\mathbf{Q}}_i^{(k)}\mathbf{U}_i^*\left(\mathbf{U}_i\mathbf{U}_i^*\right)^{-1}, \tag{23}$$

where $\mathbf{M}^*$ denotes the complex conjugate transpose of $\mathbf{M}$. Then, a normalization is applied to satisfy Eq. (16)

$$d_i^{(k+1)} = \frac{n\tilde{d}_i^{(k)}}{\sum_{j=1}^{n}|\tilde{d}_j^{(k)}|} \tag{24}$$

These updated values of the normalized calibration factors are the diagonal elements of matrix $\mathbf{D}^{(k+1)}$, which is needed to start iteration $k+1$. The iterative process can be stopped either after a fixed number of iterations, or if a convergence criterion is satisfied. The quality of the result can be assessed at each iteration by computing the snr indicator of the projection (cf. Eq. (11)):

$$\mathrm{snr}^{k+1} = 20\log_{10}\left(\frac{\|\mathbf{\Psi}\mathbf{D}^{k+1}\mathbf{U}\|_F}{\|(\mathbf{I}-\mathbf{\Psi})\mathbf{D}^{k+1}\mathbf{U}\|_F}\right) \tag{25}$$

2.5. Frequency smoothing

The calibration factors, that are to be estimated, are expected to have relatively smooth responses in the frequency domain. This expectation can be used as an a priori information to add another constraint to the optimization problem. It is proposed here to consider a linearization of the calibration factor in a frequency range around ω_0. Eq. (22) is replaced by the following equation

$$\tilde{\mathbf{Q}}_i(\omega) = (d_{i0} + (\omega-\omega_0)\gamma_{i0})\mathbf{U}_i(\omega), \tag{26}$$

where d_{i0} is the mean value of the calibration factor around the frequency ω_0 and γ_{i0} the slope. Considering this relation for a frequency range containing $2M+1$ points around ω_0, with a frequency resolution of Ω, i.e. $\omega \in [\omega_0 \pm M\Omega]$, the following system is established

$$\begin{cases} \tilde{\mathbf{Q}}_i(\omega_0 - M\Omega) = \left(\mathrm{d}_{i0} - M\Omega\gamma_{i0}\right) & \mathbf{U}_i(\omega_0 - M\Omega) \\ \vdots & \\ \tilde{\mathbf{Q}}_i(\omega_0 + M\Omega) = \left(\mathrm{d}_{i0} + M\Omega\gamma_{i0}\right) & \mathbf{U}_i(\omega_0 + M\Omega) \end{cases}, \tag{27}$$

or, in a matrix form

$$\mathbf{M_Q} = [d_{i0}\ \ \gamma_{i0}]\mathbf{M_U}$$
$$\text{with } \mathbf{M_Q} = \left[\tilde{\mathbf{Q}}_i(\omega_0 - M\Omega)\ \ \ldots\ \ \tilde{\mathbf{Q}}_i(\omega_0 + M\Omega)\right]$$
$$\mathbf{M_U} = \begin{bmatrix} \mathbf{U}_i(\omega_0 - M\Omega) & \ldots & \mathbf{U}_i(\omega_0 + M\Omega) \\ -M\Omega\mathbf{U}_i(\omega_0 - M\Omega) & \ldots & M\Omega\mathbf{U}_i(\omega_0 + M\Omega) \end{bmatrix}$$

The parameters of the calibration are then estimated using the following equation, to be used in place of Eq. (23)

$$\left[\tilde{d}_{i0}\ \ \tilde{\gamma}_{i0}\right] = \mathbf{M_Q}\mathbf{M_U}^*\left(\mathbf{M_U}\mathbf{M_U}^*\right)^{-1}. \tag{28}$$

Finally, the estimation of $\tilde{d}_{i0}$ still needs to be normalized to obtain d_{i0}, using Eq. (24).

2.6. Scaling of relative calibrations

The relative calibration factors, whose determination is discussed in the previous section, have to be scaled to obtain absolute values in Pa/V. For this purpose, the value of the scaling factor $\bar{c}$ has to be determined, at each frequency. It can be done if a part of the sensors is calibrated with another approach (typically with an individual calibration device). The following system is considered at each frequency

$$\begin{pmatrix} d_1 \\ \vdots \\ d_r \end{pmatrix} \bar{c} = \begin{pmatrix} c_1 \\ \vdots \\ c_r \end{pmatrix}, \quad \text{or} \quad \mathbf{d}_r \bar{c} = \mathbf{c}_r \tag{29}$$

where the calibration of sensors 1 to r are known (elements of $\mathbf{c}_r$), and where $\mathbf{d}_r$ is the vector of relative calibration factors of sensors 1 to r. The complex coefficient $\bar{c}$ is obtained by linear regression:

$$\bar{c} = \mathbf{d}_r' \mathbf{c}_r \left(\mathbf{d}_r' \mathbf{d}_r \right)^{-1}. \tag{30}$$

The full vector of calibration factors is finally obtained

$$\mathbf{c} = \bar{c} \mathbf{d} \tag{31}$$

3. Experimental illustration

3.1. Experimental setup

The indirect calibration technique is tested on the experimental bench of an open duct without flow. The setup is described in this section. The duct is 17 cm diameter and 4 m long; the aluminum wall thickness is 1 cm. An acoustic source is manually moved at one side of the duct opening (see Fig. 3); this produces the various configurations required by the calibration procedure. The acoustic source is a compression driver fed with a white noise signal. At the other duct end, the setup is equipped with an anechoic termination preventing from large acoustic reflections. It has been checked that the pressure fluctuations due to the source are at least 20 dB higher than the background noise at the microphone locations and in the frequency range of interest. The duct cut-off frequency is 1172 Hz; above 8.5 kHz, the number of cut-on modes is higher than the number of microphones. The array is constituted of 106 microphones. They are disseminated along the duct wall in an optimized fashion suited for duct mode decomposition. The optimization procedure is based on the idea that the determination of the modes amplitude described in Section 2.1 is facilitated if the condition number of the matrix $[\mathbf{\Phi}_a\ \mathbf{\Phi}_b]$ is minimized (cf. [21]). Among various random microphone positioning, the one with the lower condition number is kept. The distribution resulting from this optimisation procedure is drawn in Fig. 2 (left) as a function of z and θ. The condition number corresponding to this distribution is also drawn in the same figure (right), considering or not potential reflections at the termination of the duct.

The equipped area extends over 1 m in the axial direction and is located 2 m away from the source region as illustrated in Fig. 3. Data are acquired through a 128 channels PULSE system with a 56636 Hz sampling frequency. For each configuration 30 s of signal are recorded. Each microphone is embedded in a Teflon slot shown in Fig. 4. This cavity is connected to the inner duct volume by means of a pinhole with a 0.7 mm diameter. A rubber O-ring is added to prevent from flow leakage.

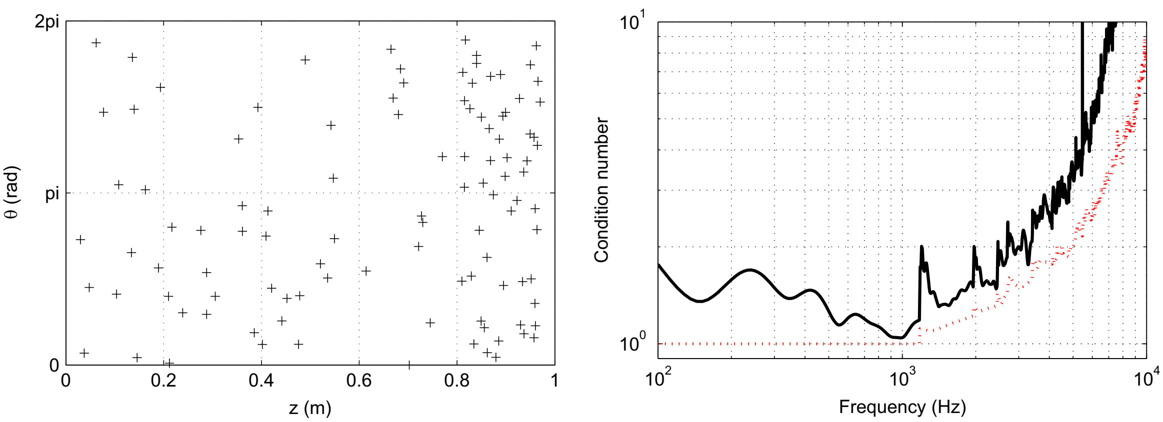

Fig. 2. Left: optimized distribution of microphones. Right: condition numbers of the corresponding modal matrices $[\mathbf{\Phi_a\Phi_b}]$ (solid black), $[\mathbf{\Phi_a}]$ (dotted red). (For interpretation of the references to color in this figure caption, the reader is referred to the web version of this paper.)

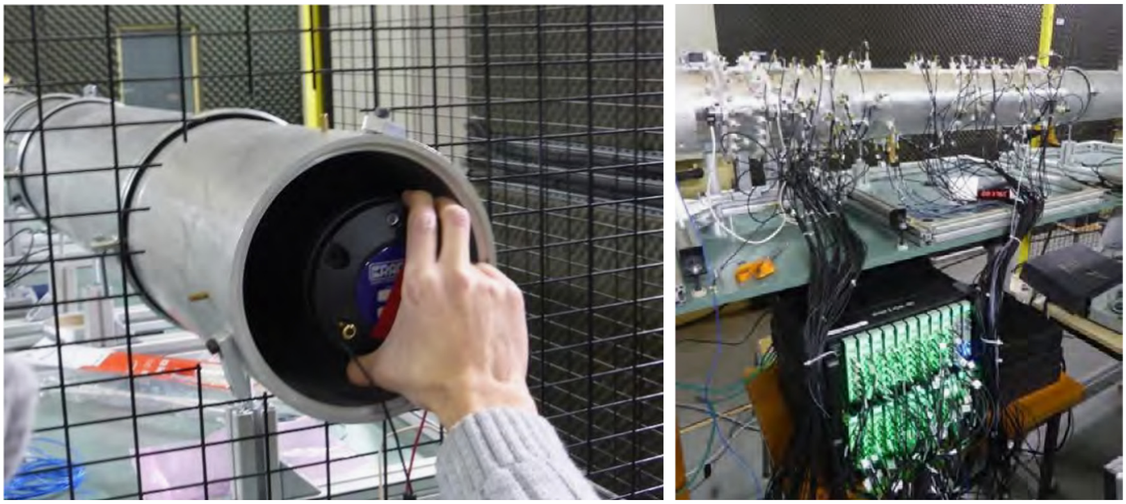

Fig. 3. Left: picture of the compression chamber placed at the duct opening. Right: picture of the duct array and the acquisition system.

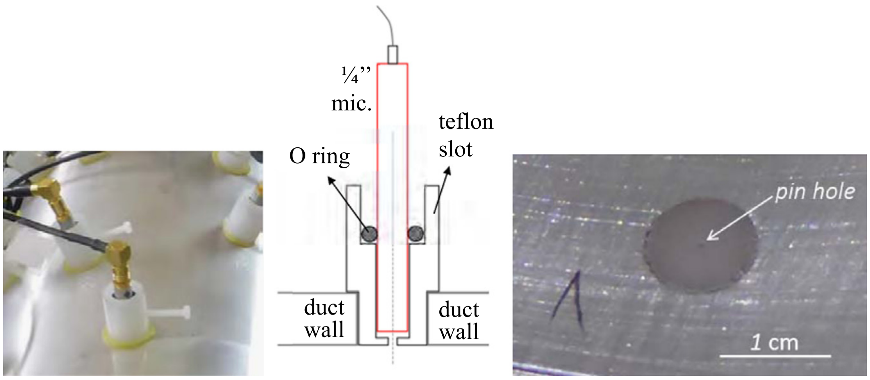

Fig. 4. Left: picture of a microphone inserted in the Teflon slot (outside view). Center: sketch of the mounting. Right: detail of the pin-hole, view from inside the duct.

With this microphone setup, the calibration function is sensitive to the microphone positioning since the cavity volume depends on the radial position of the condenser membrane. 106 Bruel & Kjaer ICP 4957 & 4958 type microphones are used.

3.2. Individual calibration system

The experimental set-up for the individual calibration system is shown in Fig. 5, and the 2 steps calibration procedure is represented in Fig. 6. In the first step, the transfer function between the reference microphone (at the outlet of the calibration system) and the microphone to be calibrated (mounted on the duct) has to be measured. To do this, the outlet of the calibration system is placed on the inner side of the duct, in front of the microphone's pin-hole, and the transfer function is measured (the compression driver delivering a broadband noise):

$$H_{ir} = S_{ri}/S_{rr}, \quad \text{in V/V} \tag{32}$$

where S_{rr} is the auto-spectrum of the reference microphone and S_{ri} the cross-spectrum between reference and the ith microphone. Both microphones are not calibrated, so the transfer function is obtained in V/V. In the second step, the calibration tube is placed on the top of a calibrated microphone on a plane baffle and the next transfer function is measured:

$$H_{cr} = S_{rc}/S_{rr}, \quad \text{in Pa/V.} \tag{33}$$

Finally, the calibration factor of microphone i is obtained as follows

$$c_i = H_{cr}/H_{ir}, \quad \text{in Pa/V.} \tag{34}$$

The procedure has been validated in terms of repeatability. However, the mounting of the microphone in the teflon slot is very sensitive, the calibration procedure should thus be repeated at each unmounting/mounting of microphones.

Fig. 5. Individual calibration system. The figure shows the driver unit connected to a flexible tube of small diameter and the reference microphone near the tube outlet.

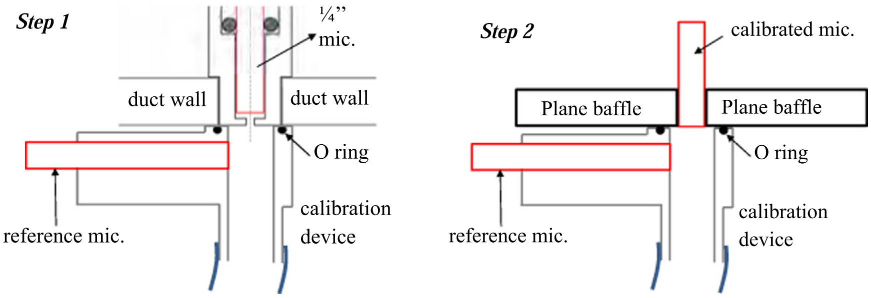

Fig. 6. Two steps individual calibration procedure. Step 1 (left): transfer function between in-duct microphone and reference microphone. Step 2 (right): transfer function between the reference microphone and the calibrated baffled microphone.

3.3. Application of the iterative calibration approach

The method described in Section 2 is applied to the bench presented in Section 3.1. The source is moved at 15 different positions around the duct's opening (source side), to consider 15 source configurations in the calibration procedure. A first position is illustrated in Fig. 3, at the center of the opening, and 14 other positions are randomly chosen on two different radii of the same section. The aim is to generate sound fields with various modal decompositions above the first cut-off frequency of the duct. For each configuration, time signals recorded by the 106 microphones are processed without any calibration to obtain a full cross spectral matrix (resolution 8 Hz, overlap 66 percent, Hanning). A principal Component analysis (cf. [22]) is then realized to extract the complex vectors $\mathbf{u}$ (one for each source configuration), in Volt, inputs of the calibration procedure. The number of propagating modes is given in Fig. 7 (left) as a function of the frequency. It can be seen that this number is equal to 2 up to 1 kHz, corresponding to the 2 plane waves travelling in both directions. Above 1 kHz, the number of propagating modes increases exponentially, up to about 140 modes at 10 kHz. It has been seen in Section 2 that the number of modes should remain lower than the number of microphones, so it is not possible to keep all modes up to 10 kHz. Thus, it is decided to keep only modes propagating from the source side towards the anechoic termination for the high frequency range (above 6 kHz). In other words, the anechoic termination is considered as fully effective above this frequency.

A frequency smoothing is implemented, as described in Section 2.5. The bandwidth used in Eq. (27), i.e. $\Delta\omega = 2M\Omega$, is defined as a function of the frequency to satisfy $\Delta\omega/\omega = 1/8$, with a lower bound $\Delta\omega_{\min} = 50$ Hz and a higher bound $\Delta\omega_{\max} = 1000$ Hz. The frequency resolution is $\Omega = 8$ Hz, the number of frequency lines considered in the smoothing operation is thus equal to 6 in low frequency and 125 in high frequency.

The signal to noise ratio of the modal projection, according Eq. (25), is drawn for each iteration in Fig. 7 (right). At iteration 1 (constant relative calibrations for all microphones), the snr lies between 5 and 15 dB. At the second iteration, the snr has already been greatly improved, by 10–20 dB below 6 kHz as compared to iteration 1. The snr above 6 kHz is also improved, by 3–5 dB. It is noteworthy that the snr is generally less good above 6 kHz, this can be explained by the fact that only propagating modes traveling from the source side are considered in that frequency range. After iteration 2, the snr continues to increase, but less significantly, and the iterative process seems to converge quite quickly: the snr reaches a maximum after about 4 iterations.

The resulting relative calibration factors are then turned into absolute ones using the procedure described in Section 2.6. 53 microphones over 106 are calibrated using the individual calibration system. The calibration factors of 10 microphones over 53 are used in Eq. (30) to estimate the scaling factor $\overline{c}$. The 43 remaining calibrated microphones are used as control points, to compare scaling factors obtained with the proposed global procedure to the ones obtained with the individual calibration system. The result of the comparison is the average calibration error, it is drawn in Fig. 8. Note that this error represents the difference between two estimates, the individual one and the global one, which are both potentially biased.

Three error curves are drawn in Fig. 8 (left), to illustrate the effect of both frequency smoothing and the multiplicity of source configurations. It is shown that it is possible to achieve a reasonable error rate, without either frequency smoothing (dotted black line) or with frequency smoothing but with only 1 source position (dashed blue). However, the best result is always obtained by considering both several source position and frequency smoothing (solid red). In the same figure (right), it is shown that the error curve is below 10 percent for 90 percent of the microphones, only few of them exhibiting errors above 15–20 percent in some frequency bands.

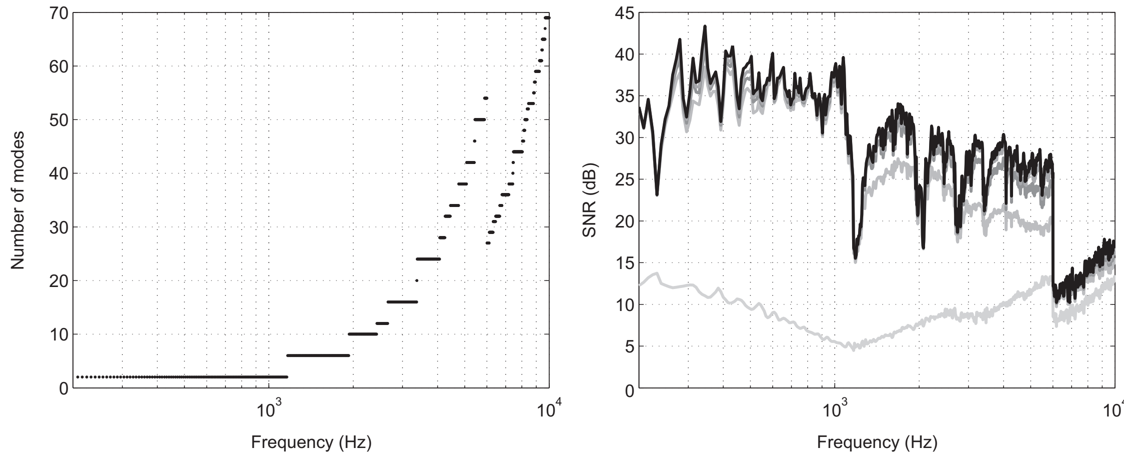

Fig. 7. Left: number of modes in the modal matrix. Right: snr of the modal projection (Eq. (25)) at each iteration from iteration 1 (light gray) to 4 (black).

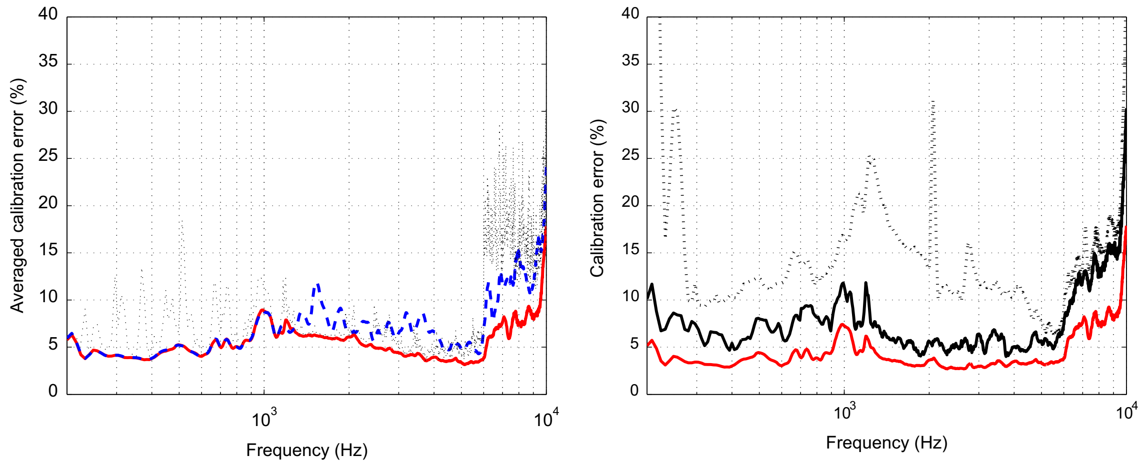

Fig. 8. Left: calibration error averaged over microphones. Dashed blue: with 1 configuration with frequency smoothing. Dotted black: with 10 configurations without frequency smoothing. Solid red: with 10 configurations and with frequency smoothing. Right: averaged calibration error (solid black), maximum calibration error (dotted black), maximum calibration error excluding 10 percent worst microphones (solid red), 10 configurations with frequency smoothing. (For interpretation of the references to color in this figure caption, the reader is referred to the web version of this paper.)

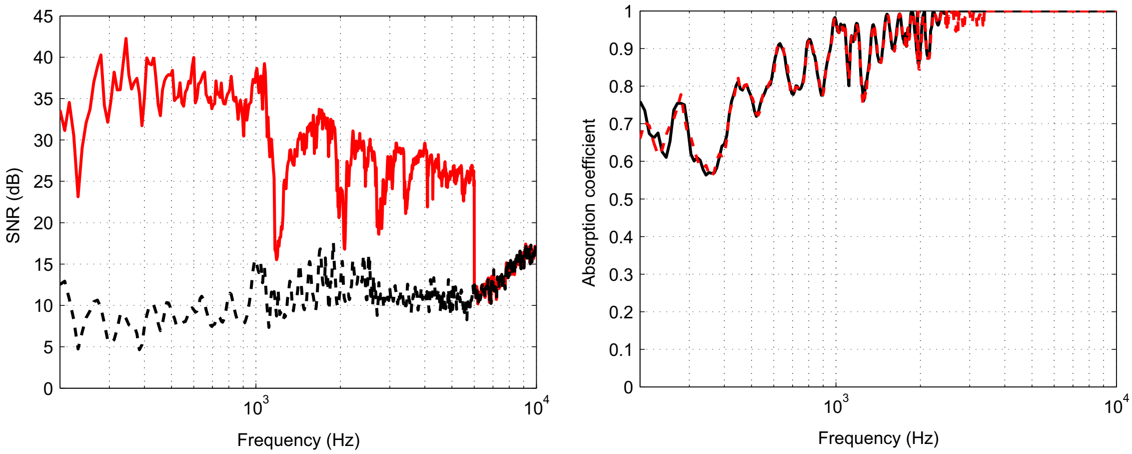

Fig. 9. Left: SNR of the modal projection, assuming no reflection (dashed black) and with potential reflection up to 6 kHz (solid red). Right: identified absorption coefficient of the duct termination for the first mode, two different source configurations. (For interpretation of the references to color in this figure caption, the reader is referred to the web version of this paper.)

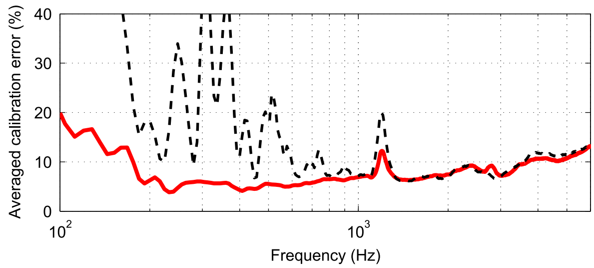

Fig. 10. Calibration error averaged over microphones. Without potential reflection (dashed black), with potential reflection (solid red). (For interpretation of the references to color in this figure caption, the reader is referred to the web version of this paper.)

3.4. Effect of considering potential reflection

The effect of considering reflections on the anechoic side of the duct is illustrated in Figs. 9 and 10. In Fig. 9 (left), the snr of the modal projection is drawn for the 4th iteration, considering propagating modes from the source side only (dashed black) and from both sides (solid red). It is clear that the snr is much better when considering both directions of wave propagation. Note that if both directions are considered, the reflection matrix can be assessed, as stated in Section 2.2. The absorption coefficient of the anechoic termination is calculated for the plane wave component and drawn in Fig. 9 (right) for two different source configurations under the assumption that the transmitted wave is fully dissipated. It is clear that this coefficient, which is found not sensitive to source positioning, is quite far from one in a wide low frequency range (up to 2–3 kHz). The calibration error (computed as for Fig. 8) with or without considering potential reflections is drawn in Fig. 10. It is clear that neglecting waves coming from the termination side is damaging for the estimation of calibration factors, at least up to 1.5 kHz.

It is noteworthy that the reflection matrix can be estimated quite precisely, using the multiplicity of source positions, as it is described in Section 2.2. This estimation can be seen as part of the bench's calibration, because the knowledge of this matrix can significantly improve the modal projection operation, by dividing by 2 the number of unknowns (see Eq. (8)).

3.5. Optimization of physical parameters: sound speed, duct radius

The global calibration procedure proposed in this work is based on the idea of finding calibration factors maximizing the adequacy between the measured duct's acoustic field, on the one hand, and an analytical modal basis on the other hand. This idea can be extended to calibrate more global parameters of the bench, like the actual sound speed (depending mainly on the temperature), and also the diameter of the duct. The final snr (obtained for the last iteration) can be estimated for a whole range of a given global parameter, and then determined as the one maximizing this indicator. This operation is conducted in the frame of this experiment, to find an optimal value of both the sound speed and duct's radius. The global snr, averaged over the whole frequency range, is drawn in Fig. 11 for the sound speed and duct radius varying between 336 and 344 m/s, and 84.6 and 85.4 mm, respectively. The effects on the snr are significant, at the order of several dB's for both parameters. Optimal values are clearly extracted, the optimal sound speed is found at 341 m/s and the optimal radius at

85.1 mm. The optimal radius may be used as is for experiments with flow, but concerning the sound speed, the optimization should be done for each measurement configuration, because of potential changes of the temperature.

3.6. Global calibration results

Some calibration factors are shown in this section as a final illustration of the procedure. Two microphones are chosen between the 43 ones that are calibrated both individually and globally, but not used at the absolute global calibration step (Section 2.6). The individual calibration of these 2 microphones is thus not used at all for the global calibration procedure. The calibration factors are drawn in Fig. 12, in modulus (left) and phase difference (right). It can be seen, firstly, that the 2 microphones have very different calibration curves, which illustrates the sensitivity to the microphone mounting (microphone positioning in its teflon slot, sealing of the mounting, etc.). However, the global shape of the theoretical response of this Helmholtz resonator-like system is well recognized, with a flat response below the acoustic mode and a frequency decreasing gain above. Secondly, it is seen in Fig. 12 that the curves obtained from the individual and global calibration procedures are in very good agreement. The results in the very low frequency range can even be supposed to be more reliable for the global approach, because of the frequency limitations of the individual system, and thanks to the frequency smoothing of the global method. The phase information of the calibration factors are presented as the phase difference between the two sensors (see right panel of Fig. 12). The difference between the 2 calibration approaches does not exceed 0.04 radians (2°) up to 10 kHz.

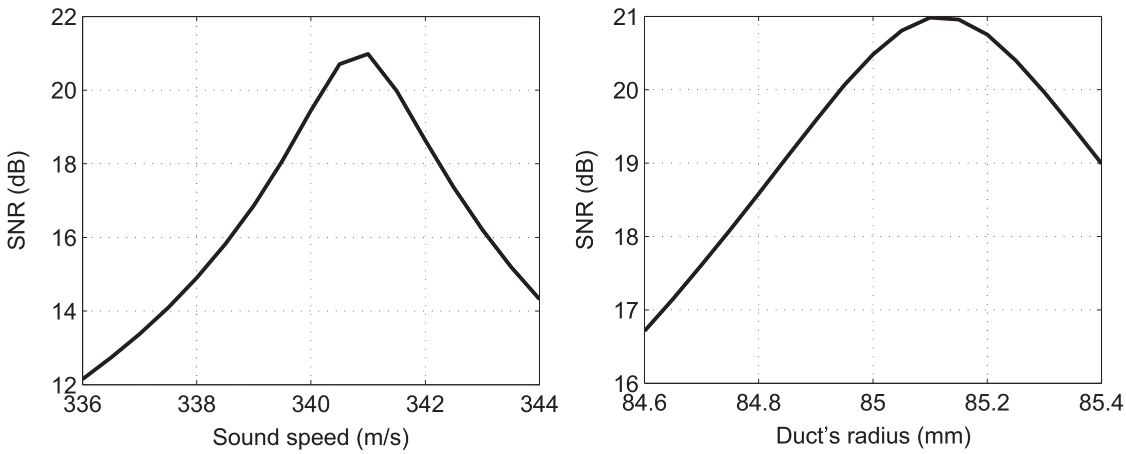

Fig. 11. Effect of numerical values assumed for the sound speed (left) and duct radius (right) on the snr of the calibration procedure.

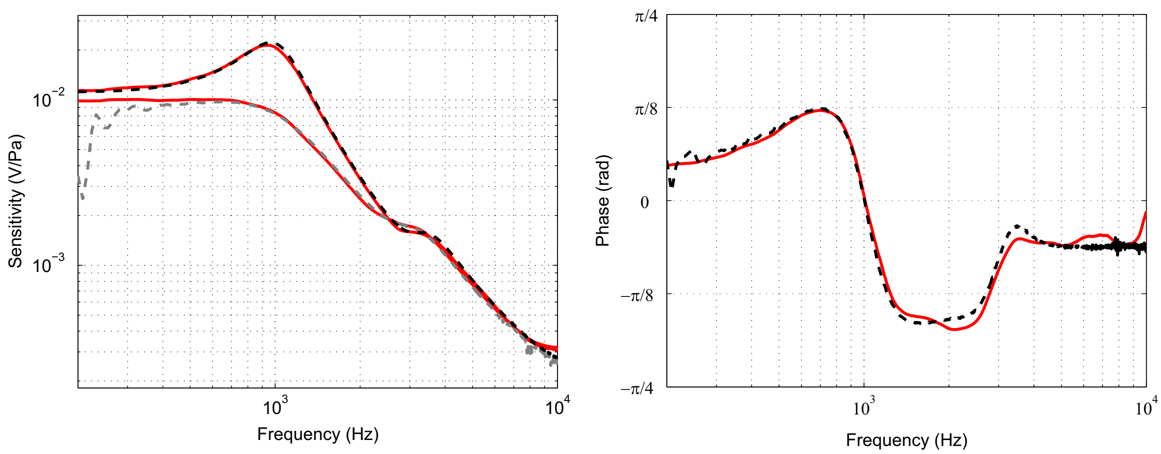

Fig. 12. Results for two different microphones. Gain in V/Pa (left), phase difference in radians between the two microphones (right). Solid red: results of the global calibration, dashed: results of individual calibrations. (For interpretation of the references to color in this figure caption, the reader is referred to the web version of this paper.)

4. Conclusions

An innovative global calibration procedure has been proposed in this paper. This procedure allows us to establish the frequency dependant microphone calibration factors of an in-duct acoustic array of any geometrical configuration, under the limitation that the modal decomposition is feasible. The procedure requires the individual calibration of few sensors, and a global calibration using an artificial source moved at several positions in the duct. A SNR indicator has been introduced to assess the quality of the result. This indicator has been found to be efficient also to calibrate more global parameters of the bench, e.g. the reflection matrix, the sound speed or the duct radius. There are perspectives for this work to be extended to more classical acoustic arrays with free field conditions, in a context where the arrays are constituted of more and more microphones, and where the quality of sensors needs sometimes to be downgraded due to cost or technological reasons.

Acknowledgments

This work was performed within the framework of the Labex CeLyA of Université de Lyon, operated by the French National Research Agency (ANR-10-LABX-0060/ANR-11-IDEX-0007), and supported by the Labcom P3A (ANR-13-LAB2-0011-01).

References

[1] F.O. Castres, P.F. Joseph, Experimental investigation of an inversion technique for the determination of broadband duct mode amplitudes by the use of near-field sensor arrays, *The Journal of the Acoustical Society of America* 122 (2) (2007) 848–859.
[2] P. Sijtsma, Feasibility of in-duct beamforming, *13th AIAA/CEAS Aeroacoustics Conference*, Rome, Italy, vol. 3696, 2007, p. 2007.
[3] U. Tapken, T. Raitor, L. Enghardt, Tonal noise radiation from an UHBR fan-Optimized in-duct radial mode analysis, *Proceedings of the 15th AIAA/CEAS Aeroacoustics Conference*, Miami, FL, USA, no. 3288, 2009.
[4] C. Lowis, P. Joseph, A. Kempton, Estimation of the far-field directivity of broadband aeroengine fan noise using an in-duct axial microphone array, *Journal of Sound and Vibration* 329 (19) (2010) 3940–3957.
[5] P. Sijtsma, Using phased array beamforming to identify broadband noise sources in a turbofan engine, *International Journal of Aeroacoustics* 9 (3) (2010) 357–374.
[6] R.P. Dougherty, B.E. Walker, D.L. Sutliff, Locating and quantifying broadband fan sources using in-duct microphones, *16th AIAA/CEAS Aeroacoustics Conference*, Stockholm, Sweden, no. 3736, 2010.
[7] M. Lee, J.S. Bolton, L. Mongeau, Application of cylindrical near-field acoustical holography to the visualization of aeroacoustic sources, *The Journal of the Acoustical Society of America* 114 (2) (2003) 842–858.
[8] A. Paulraj, T. Kailath, Direction of arrival estimation by eigenstructure methods with unknown sensor gain and phase, *IEEE International Conference on Acoustics, Speech, and Signal Processing, ICASSP'85*, Vol. 10, April 1985, pp. 640–643.
[9] Y. Sng, Y. Li, Fast algorithm for gain and phase error calibration of linear equi-spaced (LES) array, *5th International Conference on Signal Processing Proceedings, 2000, WCCC-ICSP 2000*, Vol. 1, 2000, pp. 441–444.
[10] P. Heidenreich, A. Zoubir, Gain and phase autocalibration for uniform rectangular arrays, *2011 IEEE International Conference on Acoustics, Speech and Signal Processing (ICASSP)*, May 2011, pp. 2568–2571.
[11] R.P. Dougherty, Beamforming in acoustic testing, in: T. Mueller (Ed.), *Aeroacoustic Measurements, Experimental Fluid Mechanics*, Springer, Berlin, Heidelberg, 2002, pp. 62–97.
[12] C. Lowis, P. Joseph, P. Sijtsma, A technique for the in situ phase calibration of in-duct axial microphone arrays, *Journal of Sound and Vibration* 329 (22) (2010) 4634–4642.
[13] C. Lowis, P. Joseph, An in-situ phase calibration technique for in-duct axial microphone arrays, *Proceedings of the 15th AIAA/CEAS Aeroacoustics Conference*, Miami, FL, USA, no. 3123, 2009.
[14] P. Toth, C. Schram, Simultaneous calibration of multiple microphones for both phase and amplitude in an impedance tube, *Archives of Acoustics* 39 (no. 2) (2014).
[15] G.M. Corcos, Resolution of pressure in turbulence, *The Journal of the Acoustical Society of America* 35 (2) (1963) 192–199.
[16] E. Salze, C. Bailly, O. Marsden, E. Jondeau, D. Juvé, An experimental characterization of wall pressure wavevector-frequency spectra in the presence of pressure gradients, *20th AIAA/CEAS Aeroacoustics Conference*, Atlanta, GA, no. 2909, 2014.
[17] C. Moore, Measurement of radial and circumferential modes in annular and circular fan ducts, *Journal of Sound and Vibration* 62 (2) (1979) 235–256.
[18] M. Åbom, Modal decomposition in ducts based on transfer function measurements between microphone pairs, *Journal of Sound and Vibration* 135 (1) (1989) 95–114.
[19] G.J. Bennett, C. O'Reilly, U. Tapken, J. Fitzpatrick, Noise source location in turbomachinery using coherence based modal decomposition, *Proceedings of the 15th AIAA/CEAS Aeroacoustics Conference*, Miami, FL, USA, no. 3367, 2009.
[20] M. Akoum, J.-M. Ville, Measurement of the reflection matrix of a discontinuity in a duct, *The Journal of the Acoustical Society of America* 103 (5) (1998) 2463–2468.
[21] U. Tapken, L. Enghardt, Optimisation of sensor arrays for radial mode analysis in flow ducts, *Proceedings of the 12th AIAA/CEAS Aeroacoustics Conference (27th AIAA Aeroacoustics Conference)*, Cambridge, MA, USA, 2006.
[22] S. Price, R. Bernhard, Virtual coherence: a digital signal processing technique for incoherent source identification, *Proceedings of IMAC*, Vol. 4, Schenectady, NY, USA, 1986.